ISBN: 978-3-95450-247-9 ISSN: 2673-5490 doi: 10.18429/JACoW-IPAC2024-MOPR56

DESIGN AND MODELING OF HOFI PLASMA CHANNELS FOR LASER PLASMA ACCELERATORS *

N. Cook†, S. Coleman, C. Hall, K. Wolfinger
RadiaSoft, Boulder, CO, USA
C. Benedetti, A. Gonsalves, A. Picksley, C. Schroeder
Lawrence Berkeley National Laboratory, Berkeley, CA, USA

Abstract

Structured plasma channels are an essential technology for driving high-gradient, plasma-based acceleration and control of electron and positron beams for advanced concepts accelerators. Laser and gas technologies can permit the generation of long plasma columns known as hydrodynamic, optically-field-ionized (HOFI) channels, which feature low on-axis densities and steep walls. By carefully selecting the background gas and laser properties, one can generate narrow, tunable plasma channels for guiding high intensity laser pulses. We present on the development of 1D and 2D simulations of HOFI channels using the FLASH code, a publicly available radiation hydrodynamics code with specific improvements to model plasma channels. We explore sensitivities of the channel evolution to laser profile, intensity, and background gas conditions. We examine efforts to benchmark these simulations against experimental measurements of plasma channels. Lastly, we discuss ongoing work to couple these tools to community PIC models to capture variations in initial conditions and subsequent coupling for laser wakefield accelerator applications.

INTRODUCTION

Plasma accelerators generate exceptional accelerating fields through efficient coupling of laser/beam energy into plasma waves, in turn accelerating electrons to large energies over short distances [1–3]. Although beam-based (PWFA) and laser-based (LWFA) concepts differ in their experimental configuration, they each impose requirements on controllable plasma structures for maximizing gradient, efficiency, and stability.

Recent advancements in laser technologies have identified a promising strategy for generating narrow, low-density plasma channels, referred to as hydrodynamic optical-field-ionized channels (OFI or HOFI) [4, 5]. Using novel optical configurations, a long laser focus is generated at higher peak intensity than is typical from an axicon lens [6], enabling field ionization along a narrow channel. Subsequent heating of the generated electrons by the ionizing laser drives hydrodynamic expansion of the generated plasma radially outward, producing a dynamic channel with a steeper density gradient. By carefully selecting the laser and gas parameters and the relative timing between ionizing laser and drive pulse, HOFI plasma channels may enable the formation of waveguides with unprecedented flexibility for matching laser spots well below the 60 μm level previously achieved with laser-heated capillary discharges [7].

Increasing interest in this technology has motivated the development and investigation of improved modeling tools to inform channel design [4, 8–10]. This paper outlines a hydrodynamic model that incorporates estimates of laser deposition to predict the plasma channel formation across a range of laser and gas characteristics of interest for laser plasma accelerators.

SIMULATION CONFIGURATION

Our approach adopts FLASH, a radiation magnetohydrodynamics application developed by the Flash Center for Computational Science, specializing in the simulation of high energy density plasmas (HEDP), ranging from solar phenomena to laboratory astrophysics to fusion experiments [11]. Our work builds upon experience from recent efforts with the FLASH code to develop and validate models for capillary discahrge plasmas [12].

We implemented prototype models in a 2D Cartesian geometry. The simulation configuration specifies the gas species composition, density and temperature at the start of the simulation. A tabulated equation-of-state is employed to compute internal energies as required for closure of (magneto)hydrodynamic equations as well as to provide localized ionization estimates as required for computing plasma-specific transport, most notably thermal conduction and magnetic resistivity. Adaptive mesh refinement (AMR) is employed to enable dynamic resolution enhancement in regions of large density, temperature, and pressure gradients.

LASER DEPOSITION

Here we describe the model used to estimate the ionization and subsequent thermal deposition.

The initial temperature is primarily the result of the laser's contributions to the electron momenta at the time of ionization. Because the ionization does not occur instantaneously, a self-consistent time-dependent model was generated to integrate the ionization profile of the gas over time, and to estimate the effective momentum contribution to each newly ionized component. Equation (1) relates the ionization rate in time,

* Work supported by the U.S. D.O.E.,Office of Science, Office of High Energy Physics under Award Number(s) DE-SC0024244. This work was supported by DARPA and by Office of Science, US DOE, Contract No. DE-AC02-05CH11231.
† ncook@radiasoft.net

ISBN: 978-3-95450-247-9 ISSN: 2673-5490 doi: 10.18429/JACoW-IPAC2024-MOPR56

$$\partial_t \left(\frac{n}{n_\mathrm{g}}\right) = \left[1 - \frac{n}{n_\mathrm{g}}\right] \mathrm{W}(t) \tag{1}$$

where $\mathrm{W}(t)$ is the instantaneous ionization rate, n_g is the neutral gas density, and n is the ionized plasma density. In the limit of low Keldysh parameter ($\gamma = \omega\sqrt{2\mathrm{U_I}}/\mathrm{E}$, where ω is the laser frequency, E is the laser field, and $\mathrm{U_I}$ is the ionization potential), one can compute the instantaneous ionization rate from the ADK formula,

$$W(t) = 4\frac{\alpha c}{r_\mathrm{B}}\left(\frac{U_I}{U_H}\right)^{5/2} \frac{r_e/r_\mathrm{B}^2}{e|E(t)|/\mathrm{mc}^2}\times \exp\left[-\frac{2}{3}\left(\frac{U_I}{U_H}\right)^{3/2} \frac{r_e/r_\mathrm{B}^2}{q_\mathrm{e}|E(t)|/\mathrm{mc}^2}\right] \tag{2}$$

where U_H is the first ionization potential of Hydrogen (13.6 eV), λ_i is the ionizing laser wavelength, $\alpha = e^2\hbar c$ is the fine structure constant, q_e is the electron charge, r_e is the classical electron radius, and r_B is the Bohr radius.

The effective momentum transfer is a function of the laser normalized intensity, a, and polarization at the time of ionization. For a linearly polarized pulse near threshold intensity, the momentum transfer is therefore suppressed owing to the phase mismatch between the electric field, responsible for the local ionization, and the vector potential, responsible for the momentum transfer. If the laser field can be fully resolved, then the resulting momentum transfer is simply $p_{x_i}(t) = ma_i(t)$. For an elliptically polarized pulse, the momentum transfer in each plane is a function of the planar vector potential contributions, e.g., $p_{x_i,y_i}(t) = ma_{x_i,y_i}(t)$. The corresponding planar kinetic energy transfer is a function of the rms momentum spread in the ionized electrons, via

$$K_\mathrm{x,y} = \frac{1}{2} m_e c^2 a^2_{x_i,y_i} \tag{3}$$

Finally, thermalization of the electrons necessitates the redistribution of planar momentum to all degrees of freedom. Again, this is a polarization-dependent process, as linearly polarized pulses transfer momentum in a single plane, whereas circularly polarized pulses transfer momentum in both planes.

$$\mathrm{T} = \sum_\mathrm{x,y} K_\mathrm{x,y}/3q_\mathrm{e} \tag{4}$$

We conclude that both intensity and polarization play essential roles in the temperature estimate. Linearly polarized pulses provide the lowest heating quotient to the plasma, while circularly polarized pulses provide the highest. Intermediate polarization can be used to scan intermediate temperatures. However, we note that the ionization rate, being dependent on the peak field, is reduced in the presence of circular polarization, as the field is distributed in two planes and reaches a peak of $\sqrt{2}/2$ times the peak field with linear polarization, for the same pulse energy, width, and duration. Figure 1 shows a comparison of the radial ionization and temperature profiles computed using the procedure described above.

RESULTS & DISCUSSION

With these models in place, we explored the deposition scalings as a function of intensity for the Bessel beam configuration, including polarization contributions. We considered three figures of merit: (i) peak on axis temperature, (ii) radial extent of deposition, and (iii) effective linear energy deposition (e.g., dE/dz), which serves as a composite indicator of how much energy is being deposited in a transverse slice of gas. Figure 2 depicts the peak temperature scaling, which shows good agreement with predicted scalings and simulated results from previous studies [9, 13]. At high intensities, peak temperatures begin to rise more rapidly near the laser axis.

Figure 3 depicts the radial extent. The radial extent is characterized in two ways: the location at which ionization exceeds 1%, and the location at which the temperature increases by roughly a factor of 2 from room temperature. We note that for linear polarizations, there is a modest gap between these two locations, as ionization precedes heating on the intensity scale, whereas for circular polarization, ionization is suppressed while heating is enhanced, and the two metrics overlap.

Both plots show the effective linear deposition, computed by integrating the temperature distribution and weighting by the density and heat capacity. It can be seen that the linear deposition scales more closely with the peak temperature at low intensities, but continues to rise even after the peak temperature flattens out due to the increased cross-sectional area of the deposition. This dramatic increase in deposition at higher intensities is a unique signature of the Bessel beam, as the cross-sectional area of each additional ring is significantly larger than the previous one.

With these models in place, we've simulated numerous channel configurations to explore parameter spaces consistent with recent experimental configurations from the BELLA PW laser system. Figure 4 depicts a result using a Bessel beam with characteristic size consistent with the one employed at BELLA, and using linear polarization and a normalized intensity of $a_0 \approx 0.05$. We note the competing influence of thermal diffusion and channel expansion at early timescales introduce significant variations in the underlying channel density at low timescales. At longer times, the temperature variations diminish, and the resulting channel shows smoothly varying density. Another characteristic of the Bessel deposition profile is the introduction of secondary blast wave features that generate time-varying channel wall thickness. We are continuing to evaluate these characteristics against recent measurements to validate this behavior and identify optimal operating conditions for future experiments.

ISBN: 978-3-95450-247-9 ISSN: 2673-5490 doi: 10.18429/JACoW-IPAC2024-MOPR56

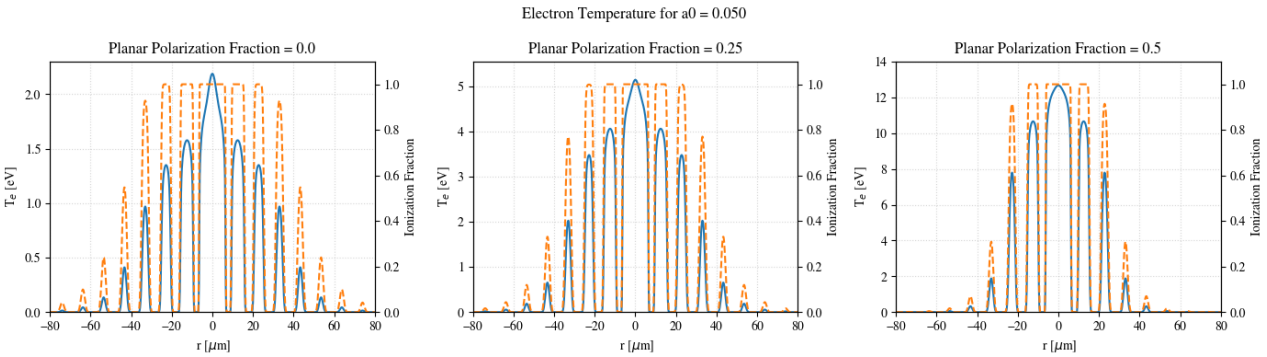

Figure 1: Ionization and temperature profiles for varying ellipticities, range from 0 (linear) to 0.5 (circular) polarization.

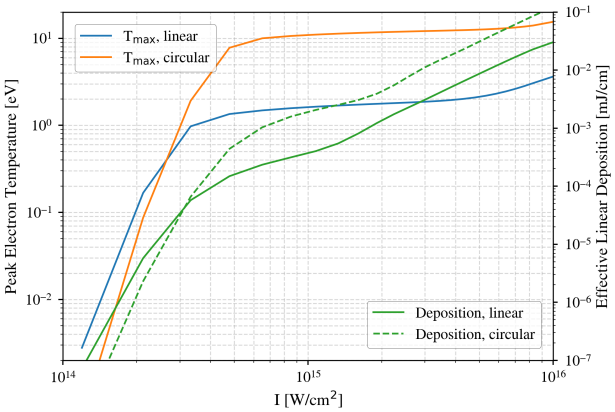

Figure 2: Peak temperature as a function of intensity for linear and circularly polarized pulses. Note that the temperature plateaus and is only weakly dependent on intensity above threshold.

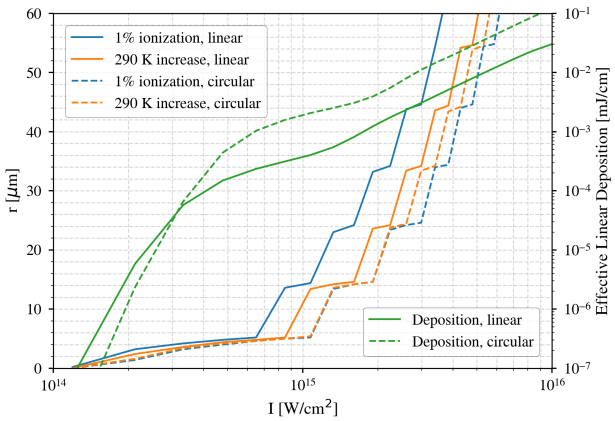

Figure 3: Radial extent of ionization as a function of intensity for linear and circular polarization. Sharp increases are seen with the addition of each additional ring in the Bessel profile.

CONCLUSION

We have presented a hydrodynamic model for capturing the dynamics of hydrodynamic optical-field ionized plasma channels for use with laser plasma acceleration. Specific attention is paid to the estimation of initial electron temperature profiles resulting from the interaction of an intense Bessel-Gaussian laser pulse. Estimated initial temperatures as a function of intensity show good agreement with previous work. The Bessel distribution introduces significant variation in deposited energy as a function of intensity, especially away from the laser axis. This deposition pattern introduces non-trivial temporal correlations that may have significance in determining optimal intensity and delay settings for use with accelerators. Ongoing work seeks to validate these models against experimental measurement leveraging two color interferometry.

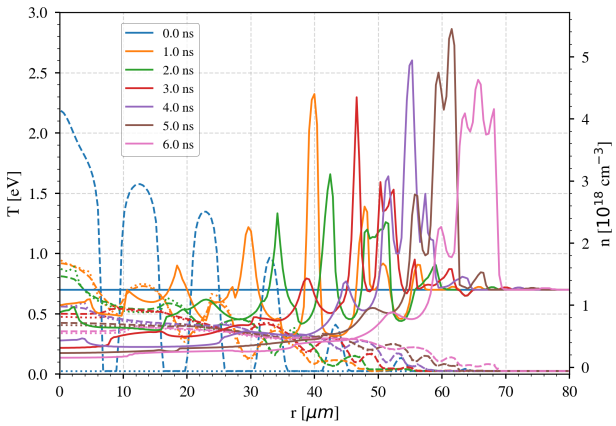

Figure 4: Density (solid) and electron temperature (dashed) sampled across the first 6 ns of evolution following the interaction of a linearly polarized Bessel beam with $a_0 \approx 0.05$.

ACKNOWLEDGMENTS

This material is based upon work supported by the U.S. D.O.E.,Office of Science, Office of High Energy Physics under Award Number(s) DE-SC0024244. This work was supported by DARPA and by Office of Science, US DOE, Contract No. DE-AC02-05CH11231.

REFERENCES

[1] P. Chen, J. M. Dawson, R. W. Huff, and T. Katsouleas, "Acceleration of electrons by the interaction of a bunched electron

ISBN: 978-3-95450-247-9 ISSN: 2673-5490 doi: 10.18429/JACoW-IPAC2024-MOPR56

beam with a plasma," *Phys. Rev. Lett.*, vol. 54, no. 7, pp. 693–696, 1985. doi:10.1103/PhysRevLett.54.693

[2] E. Esarey, P. Sprangle, J. Krall, and A. Ting, "Overview of plasma-based accelerator concepts," *IEEE Trans. Plasma Sci.*, vol. 24, no. 2, pp. 252–288, 1996. doi:10.1109/27.509991

[3] E. Esarey, C. B. Schroeder, and W. P. Leemans, "Physics of laser-driven plasma-based electron accelerators," *Rev. Mod. Phys.*, vol. 81, no. 3, pp. 1229–1285, 2009. doi:10.1103/RevModPhys.81.1229

[4] R. J. Shalloo *et al.*, "Hydrodynamic optical-field-ionized plasma channels," *Phys. Rev. E*, vol. 97, no. 5, p. 053 203, 2018. doi:10.1103/PhysRevE.97.053203

[5] B. Miao, L. Feder, J. E. Shrock, A. Goffin, and H. M. Milchberg, "Optical guiding in meter-scale plasma waveguides," *Phys. Rev. Lett.*, vol. 125, no. 7, p. 074 801, 2020. doi:10.1103/PhysRevLett.125.074801

[6] S. Smartsev *et al.*, "Axiparabola: A long-focal-depth, high-resolution mirror for broadband high-intensity lasers," *Opt. Lett.*, vol. 44, no. 14, pp. 3414–3417, 2019. doi:10.1364/OL.44.003414

[7] A. J. Gonsalves *et al.*, "Petawatt laser guiding and electron beam acceleration to 8 gev in a laser-heated capillary discharge waveguide," *Phys. Rev. Lett.*, vol. 122, no. 8, p. 084 801, 2019. doi:10.1103/PhysRevLett.122.084801

[8] A. Picksley *et al.*, "Guiding of high-intensity laser pulses in 100-mm-long hydrodynamic optical-field-ionized plasma channels," *Phys. Rev. Accel. Beams*, vol. 23, no. 8, p. 081 303, 2020. doi:10.1103/PhysRevAccelBeams.23.081303

[9] S. M. Mewes *et al.*, "Demonstration of tunability of hofi waveguides via start-to-end simulations," *Phys. Rev. Res.*, vol. 5, no. 3, p. 033 112, 2023. doi:10.1103/PhysRevResearch.5.033112

[10] B. Miao, E. Rockafellow, J. E. Shrock, S. W. Hancock, D. Gordon, and H. M. Milchberg, *Benchmarking of hydrodynamic plasma waveguides for multi-gev laser-driven electron acceleration*, 2024.

[11] P. Tzeferacos *et al.*, "Flash mhd simulations of experiments that study shock-generated magnetic fields," *High Energy Density Physics*, vol. 17, pp. 24–31, 2015. doi:https://doi.org/10.1016/j.hedp.2014.11.003

[12] A. Diaw, S. J. Coleman, N. M. Cook, J. Edelen, E. C. Hansen, and P. Tzeferacos, "Impact of Electron Transport Models on Capillary Discharge Plasmas," *arXiv e-prints*, paper arXiv:2203.09569, arXiv:2203.09569, 2022. https://ui.adsabs.harvard.edu/abs/2022arXiv220309569D

[13] C. B. Schroeder *et al.*, "Thermal emittance from ionization-induced trapping in plasma accelerators," *Phys. Rev. Spec. Top. Accel. Beams*, vol. 17, no. 10, p. 101 301, 2014. doi:10.1103/PhysRevSTAB.17.101301